Hindawi
International Transactions on Electrical Energy Systems
Volume 2022, Article ID 1951836, 20 pages
https://doi.org/10.1155/2022/1951836

Research Article

Assessment of the Phase-to-Ground Fault Apparent Admittance Method with Phase/Ground Boundaries to Detect Types of Electrical Faults for Protective Relays Using Signature Library and Simulated Events

Emilio C. Piesciorovsky[1] **and Marissa E. Morales Rodriguez**[2]

[1]*Power Systems Resilience Group, Electrification and Energy Infrastructures Division, Oak Ridge National Laboratory, Oak Ridge, Tennessee 37830, USA*
[2]*Solar Energy Technologies Office, US Department of Energy, Washington D.C. 20585, USA*

Correspondence should be addressed to Emilio C. Piesciorovsky; emiliopiesciorovsky@hotmail.com

Received 24 March 2022; Revised 6 June 2022; Accepted 28 June 2022; Published 26 September 2022

Academic Editor: Sheng Du

Protective relays in electric power grids recognize the types of electrical faults in a few seconds. The most common detection method to detect the types of electrical faults is based on measuring the angle between the zero and negative sequence currents. However, it is not completely accurate because the phase-to-phase-ground and phase-to-ground electrical faults could have the same detection conditions. Therefore, engineers need to plot the events after an electrical fault to observe the nature of the incidents in detail. In this study, the phase-to-ground fault apparent (PGFA) admittance method with phase/ground boundaries identified the types of electrical faults located in distribution power lines and feeders. This method was based on measuring the PGFA admittance magnitudes for the faulted and nonfaulted phases, resulting in greater than zero and near zero, respectively. The PGFA admittance algorithm was built with MATLAB/Simulink software and tested with signature library and grid simulation events. The PGFA method with phase/ground boundaries was evaluated with the confusion matrix. The measured and predicted values matched in more than 90% of the tests, and the PGFA admittance method with phase/ground boundaries presented an accuracy of 94.3% and a precision of 100%.

1. Introduction

Protective relays can detect breaker states [1, 2], types of electrical faults [3, 4], and fault locations [5–7] in a few seconds. Different protection functions [8] of relays are available for a variety of applications such as to trip/close breakers [9], to locate electrical faults in power grids or lines [10], and detecting faulted phases [4]. Protective relays have front panels with light-emitted diodes (LEDs) that represent the ground and A, B, and C phase states to identify the types of electrical faults [11]. These target LEDs are operated in a latching mode, and when a trip occurs, the electrical fault identification process begins approximately one cycle later the electrical fault identification is complete. Then, once the electrical fault identification is defined, the front panel targets are activated based on the electrical fault identification and latched on until the relay target reset push button or target reset command or target reset equation clears the targets [11]. Also, the protective relay captures the waveform data on every trip event, and the electrical fault summary is stored in the memory of the protective relay. These data can be collected to review the event history and determine the electrical fault target LEDs even after they have been cleared by the resets [11]. The detection of the types of electrical faults by a protective relay with target LEDs [12] is the first approach for protection engineers to observe the nature of events when an electrical fault occurs.

The electrical fault identification in most protective relays has been based on measuring both phase voltage and current magnitudes along with their angles. The detection of the faulted phases to observe the types of electrical faults could be performed by measuring the overcurrent magnitudes at each phase because current magnitudes usually increase at fault states. In electrical fault scenarios at microgrids, with the power grid connected or islanded to hydropower sources (high spinning inertia cases), overcurrent relays could detect the faulted phases; however, the faulted phases could not be sensed by overcurrent relays in microgrids with small diesel generators, wind turbines, and photovoltaic (PV) panels without energy storage systems (low spinning inertia cases), because of the small electrical fault currents contributed by the low inertia of distributed energy sources [13]. In addition, the most common electrical faults such as the phase to ground could be detected by measuring the voltage magnitudes, which usually decrease at faulted phases along the power line sections [14]. Considering that current and voltage magnitudes could increase and decrease, respectively, at faulted phases, the ratio between the measured phase voltages and currents at the power line sections or impedances could be used to detect the types of electrical faults.

The most important methods for detecting the types of electrical faults are based on the state of the art, because they are focused on several innovations applied on measuring the impedances [4] and sequence currents at the relay locations [3]. The computationally efficient distance relay for power transmission line [15] method measures the impedance of the electrical fault loops for multiple zones of distance protection elements. In another way, the electrical fault identification system for use in protective relays for power transmission line [16] method measures the angle between the negative and zero sequence currents, and it is based on an electrical fault identification selection logic that allows to select the types of electrical faults [16]. The detection of the types of electrical faults using the angle between the negative and zero sequence phase currents is not completely accurate because it could have the same conditions for different electrical faults [3]. In this method, the phase A to ground (AG)/phase B-C to ground (BCG) electrical faults, phase C to ground (CG)/phase A-B to ground (ABG) electrical faults, and phase B to ground (BG)/phase C-A to ground (CAG) electrical faults have an angle of 0°, 120°, and −120°, respectively [3]. Based on that, the same angle between the negative and zero sequence currents is generated for different types of electrical faults [3]. Therefore, protection engineers need to observe the relay events after an electrical fault to detect the nature of incidents in detail [17, 18], and this identification process takes a significant amount of time.

In this study, the phase-to-ground fault apparent (PGFA) admittance with phase/ground boundaries was implemented to detect the types of electrical faults at 12.47/46 kV power lines and feeders. The PGFA impedance is usually measured by the distance elements for mho relays [19, 20], which are commonly set by referring to a resistance-reactance (R-X) diagram. This diagram represents the variation over time of the impedance of the transmission line [21] at the relay location (apparent impedance). Then, the PGFA impedance algorithm from Piesciorovsky and Tarditi [22] was modified to measure the inverse of impedance (admittance) magnitudes, to detect the types of electrical faults for the A, B, and C phases, by also adding a phase/ground detection logic block. The justifications of the PGFA admittance method with phase/ground boundaries and assessment to detect the types of electrical faults were based on the current situations and resulting in the novelties shown in Table1.

The PGFA admittance method with phase/ground boundaries was evaluated to detect the types of electrical faults by using the grid simulation and signature library event modes. The assessment of protective relay algorithms is usually performed with software simulations and models that represent the ideal current and voltage sensors with relays in the loop [23, 24]. Then, simulated electrical fault currents are not affected by the saturation of measurement transformers as they would be in a real scenario. In this study, the PGFA admittance model was evaluated with the MATLAB/Simulink software and using saturated measurement transformer models [25], at the 12.47 kV Riverside—EPB of Chattanooga utility grid. On the other side, optical power line sensors were not available in MATLAB/Simulink libraries. Then, signature library events consisted of multiple real data sets collected on the field at the 46 kV EPB of Chattanooga electrical substation were applied to assess also the PGFA admittance model.

2. Methodology

2.1. Phase-to-Ground Fault Apparent Admittance with Phase/Ground Boundaries. In this research, the PGFA admittance method with phase/ground boundaries was implemented. This method focused on measuring the admittance (inverse impedance) magnitude to detect the types of electrical faults. Then, the phase to neutral voltages and phase currents at a breaker location were collected to calculate the PGFA admittance magnitude during the faulted and nonfaulted states. Distance protection relays measure the apparent impedances to detect the electrical faults in transmission lines. Considering the A phase, for instance, the PGFA impedance (Z_{ag}) was computed based on the instantaneous voltages and currents [26] by the following equation.

$$Z_{ag} = \frac{V_a}{I_a + K_0\left(3I_0\right)} = \frac{V_a}{I_a + k_0\left(I_a + I_b + I_c\right)}, \tag{1}$$

where Z_{ag} is the PGFA impedance for phase A in ohms, V_a is the phase A to neutral voltage in volts, I_a is the phase A current in amps (and similarly for I_b and I_c), $I_0 = (I_a + I_b + I_c)/3$ is the zero sequence current in amps, and K_0 is the total zero sequence current compensation factor [26]. The total zero sequence current compensation factor (K_0) is given by the following equation.

$$K_0 = \frac{Z_{T0} - Z_{T1}}{3Z_{T1}}, \tag{2}$$

Table 1: Novelties of the PGFA admittance method with phase/ground boundaries and assessment.

	Current situations (justifications)	In this study (novelties)
Methods	The sequence method used by relays has the same detection condition for the AG/BCG, CG/ABG, and BG/CAG electrical faults [3].	The PGFA admittance method with phase/ground boundaries differentiated between the AG, BCG, CG, ABG, BG, and CAG electrical faults.
	Engineers need to collect the events from the protective relays to know the nature of the electrical faults.	The PGFA admittance method with phase/ground boundaries provided a fast and reliable way to detect the types of electrical faults at medium voltage distribution power lines and feeders.
	The actual methods for detecting the types of electrical faults [4] are based on measuring the phase loop impedances [15] and positive/negative sequence currents [16].	The proposed method for detecting the types of electrical faults is based on measuring admittances with phase/ground boundaries.
Assessment	MATLAB/Simulink does not provide a complete library of the current/voltage optical power line sensors and/or saturated measurement transformers.	[(a)]MATLAB events were based on saturated measurement transformer models (MATLAB/Simulink), at the 12.47 kV Riverside—EPB of Chattanooga utility grid. [(b)]MATLAB events were based on current and voltage signals from optical power line sensors deployed on the field, at the 46 kV EPB of Chattanooga electrical substation.

[(a)]grid simulation mode and [(b)]signature library mode.

where Z_{T0} and Z_{T1} are total zero and positive sequence impedances in ohms, respectively, and expressed in standard complex notation with i as the imaginary unit.

The magnitude ($|K_0|$) and angle ($K_{0<}$) of the zero sequence current compensation factor for the power line sections were used to set the PGFA admittance algorithm. Then, $|K_0|$ and $K_{0<}$ were calculated by following equations, respectively.

$$|K_0| = \left|\frac{Z_{T0} - Z_{T1}}{3Z_{T1}}\right|, \tag{3}$$

$$K_{0<} = \tan^{-1}\left(\frac{K_{0\,\text{imag}}}{K_{0\,\text{real}}}\right), \tag{4}$$

where $K_{0\text{imag}}$ and $K_{0\text{real}}$ are the imaginary and real part of the zero sequence current compensation factor magnitude.

The total resistance (R_T) was calculated with the total positive (R_{T1}) and zero sequence resistance (R_{T0}) of the power line sections and following equation.

$$R_T = R_{T1} + R_{T2} + R_{T0} = 2R_{T1} + R_{T0}. \tag{5}$$

The total reactance (X_T) was calculated with the total positive (X_{T1}) and zero sequence (X_{T0}) reactance of the power line sections and following equation.

$$X_T = X_{T1} + X_{T2} + X_{T0} = 2X_{T1} + X_{T0}. \tag{6}$$

The total zero sequence current compensation factor magnitude ($|K_0|$) and angle ($K_{0<}$) were used to set the PGFA admittance algorithm. The total ($|Y_T|$) and zero sequence ($|Y_{T0}|$) admittance magnitudes were used to select the faulted phase and ground conditions, respectively. The $|Y_T|$ was calculated with the total resistance (R_T) and reactance (X_T) of the power line sections and following equation.

$$|Y_T| = \left|\left(\frac{R_T}{R_T^2 + X_T^2}\right) + i\left(\frac{-X_T}{R_T^2 + X_T^2}\right)\right|. \tag{7}$$

The $|Y_{T0}|$ was calculated with the total zero sequence resistance (R_{T0}) and reactance (X_{T0}) of the power line sections and following equation.

$$|Y_{T0}| = \left|\left(\frac{R_{T0}}{R_{T0}^2 + X_{T0}^2}\right) + i\left(\frac{-X_{T0}}{R_{T0}^2 + X_{T0}^2}\right)\right|. \tag{8}$$

The boundaries of the PGFA admittance method to detect the types of electrical faults with the protective relay's LEDs were defined by the phase and ground faulted zones. Then, the A, B, and C phase and ground faulted zones were set by $|Y_T|$ and $|Y_{T0}|$, respectively. The A, B, and C phase faulted zone for the measured PGFA admittance magnitudes was given by equation (7) in siemens,

$$|Y_{pg}| > |Y_T| \,(\text{phase faulted zone}), \tag{9}$$

and the ground faulted zone for the measured PGFA admittance magnitudes was given by equation (8) in siemens,

$$|Y_{pg}| > |Y_{T0}| \,(\text{ground faulted zone}). \tag{10}$$

Figure 1 shows the PGFA admittance algorithm to detect the types of electrical faults, with the data collection (1), calculation (2), measurement (3), phase condition (4), and ground condition (5) steps. The total impedance magnitudes of the zero ($|Z_{T0}|$), positive ($|Z_{T1}|$), and negative ($|Z_{T2}|$) sequences of the power line sections were used to set the calculations. The phase currents (I_A, I_B, and I_C) and phase-to-ground voltages (V_A, V_B, and V_C) were measured to calculate the magnitudes of the PGFA admittance for the A, B, and C phases, and to detect the types of electrical faults based on the phase and ground conditions for the protective relay's LEDs (Figure 1).

The PGFA admittance magnitude for a generic phase p was given by the following equation.

$$|Y_{pg}| = \left|\left(\frac{V_p}{I_p + |K_0|(I_A + I_B + I_C)}\right)^{-1}\right|. \tag{11}$$

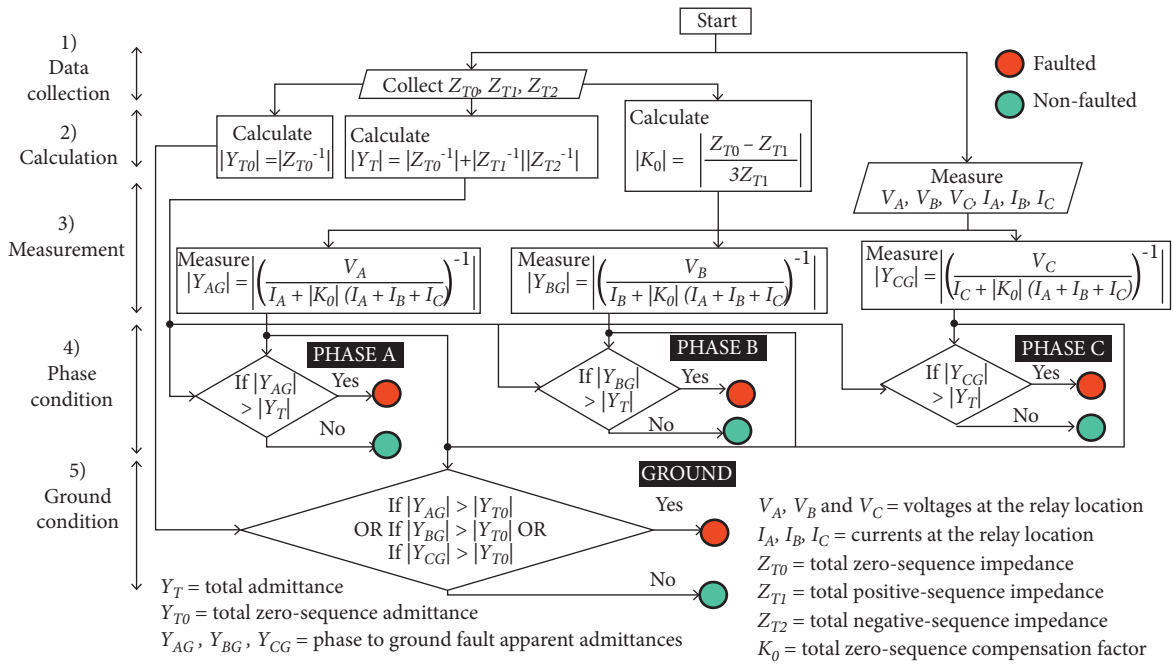

Figure 1: PGFA admittance with phase/ground boundaries to detect the types of electrical faults.

However, another way to represent the admittance is by the following equation.

$$Y_{pg} = \left|Y_{pg}\right|\cos\vartheta_{pg} + i\left|Y_{pg}\right|\sin\vartheta_{pg}, = G_{pg} + i\,B_{pg}, \tag{12}$$

where Y_{pg} is the measured PGFA admittance in siemens, G_{pg} is the measured PGFA conductance in siemens, B_{pg} is the measured PGFA susceptance in siemens, and θ_{pg} is the measured angle of the PGFA admittance in degrees.

3. Test Scenario

3.1. Flowchart of Test Scenarios. The PGFA admittance algorithm was built with the MATLAB/Simulink software. The tests were based on using two different utility grids at the Electric Power Board (EPB) of Chattanooga: the signature library event mode using the 46 kV EPB of Chattanooga electrical substation and the grid simulation mode using the 12.47 kV Riverside—EPB of Chattanooga utility grid. The signature library mode measured the currents and voltages (26.6 kV phase-to-ground voltage) from the optical power line sensors, and the grid simulation mode collected the currents and voltages (7.2 kV phase-to-ground voltage) from saturated measurement transformer models in MATLAB/Simulink. The flowchart of test scenarios to evaluate the PGFA admittance method with phase/ground boundaries is presented in Figure 2. The test scenarios were based on using the signature library and grid simulation modes, by running a selected event and simulation test, respectively. The PGFA admittance magnitude for the faulted and nonfaulted phases was measured, resulting in greater than zero and near zero, respectively.

In the signature library mode (left side of Figure 2), four sensor events were selected from Table 2, and one sensor event was downloaded in the MATLAB workspace, and the simulation for this event was run. In this case, the overcurrent relay did not trip because the stored events were read. While currents and voltages of the signature library event were being read, the PGFA admittance magnitudes for the A, B, and C phases were plotted, observing the faulted and nonfaulted phases. In the grid simulation mode (right side of Figure 2), the events were generated by the simulation of the 12.47 kV Riverside—EPB of Chattanooga utility grid in MATLAB/Simulink. Because the power grid was known, the total and zero sequence impedances and zero sequence current compensation factor were set for the PGFA admittance algorithm. Then, the electrical fault location and type of electrical fault were selected, and the simulation time was set to run the tests. In this case, the overcurrent relay tripped because the prefault, fault, and postfault states were generated for each event. The trip signal of the overcurrent relay was used to keep the measured PGFA admittance magnitude of the fault state during the postfault state. Currents and voltages of the grid simulation were generated, and the PGFA admittance magnitudes for the A, B, and C phases were plotted, observing the faulted and nonfaulted states.

3.2. Signature Library Event Mode. In the signature library event mode, the phase currents and voltages were collected from optical power line sensors (26.6 kV phase to neutral voltage) deployed on the field. The optical power line sensors were installed at the 46 kV EPB of Chattanooga electrical substation. Initially, the optical power line sensor events were stored into a signature library as COMTRADE files to be used for evaluating the PGFA admittance algorithm. Then, the phase current/voltage events from the optical

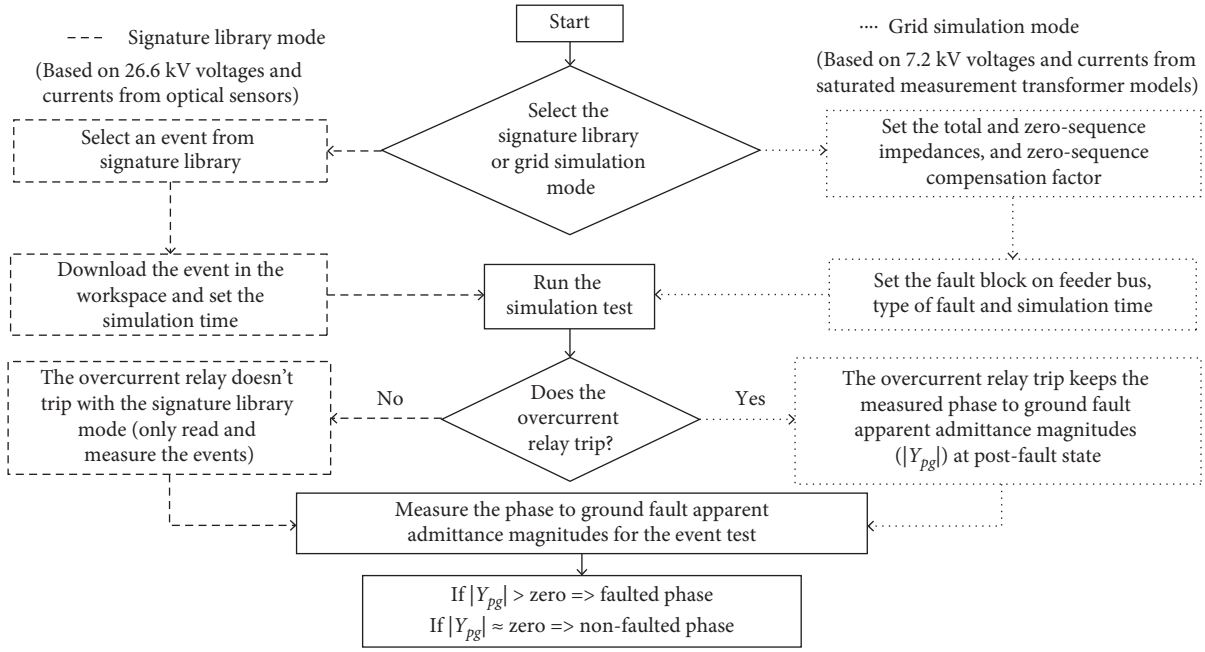

Figure 2: Flowchart of test scenarios.

Table 2: Signature library events and states.

Names	Types of tests (states)	Sensors
SIGID-931	Service restoring of A, B, and C phase feeders (nonfault state)	Optical power line sensor (26.6 kV phase to neutral voltage) for measuring phase currents and voltages
SIGID-932	Phase C to ground electrical fault that blows fuse (postfault state)	
SIGID-933	Phase C to ground electrical fault that blows fuse (postfault state)	
SIGID-934	Phase B to ground electrical fault (prefault, fault, and postfault states)	

power line sensors were converted into MATLAB files to be used with the PGFA admittance algorithm. These signature library events were given by a service restoring of A, B, and C phase feeders, phase C to ground fault that blows fuse (postfault state), and phase B to ground fault (prefault, fault, and postfault states). The BG fault event (SIGID-934) included the effect of the fault resistance because it was collected from a real power system operated by the Electrical Power Board (EPB) utility of Chattanooga. The effect of load switching was represented by the service restoring of A, B, and C phase feeders' event (SIGID-931) that represents a nonfault state situation. Table 2 shows the signature library events.

3.3. Grid Simulation Event Mode. In the grid simulation event mode, part of the 12.47 kV Riverside—EPB of Chattanooga utility grid[13]—was simulated with MATLAB/Simulink software. The single-line diagram of the power grid circuit is shown in Figure 3, and this network configuration was a radial power system (7.2 kV phase-to-ground voltage) that was fed by a three-phase source with a Wye-ground configuration (Riverside substation). In this study, the overcurrent relay with the PGFA admittance algorithm was located between the power line sections 27 and 28, to detect the faulted phases for the line-to-ground (LG), double-line-to-ground (LLG), line-to-line (LL), three-line (3L), and three-line-to-ground (3LG) electrical faults located near the relay's breaker and at the end of the power line sections 28 and 38.

Figure 4 shows the three-line diagram for the MATLAB/Simulink model with the (a) power grid circuit, (b) breaker, (c) inverse time overcurrent relay, (d) fault block circuit, (e) fault block, (f) current and (g) potential transformers, and (h and j) fault locations. This power grid circuit (Figure 4(a)) included the utility source, power line sections, feeder loads, breakers, and capacitor banks. The power line sections were simulated with a three-phase π section line block. The electrical faults were generated by a fault block (Figure 4(e)) operated by the fault block circuit (Figure 4(d)) that tripped the electrical fault state at 0.5 s. The LG, LL, LLG, 3L, and 3LG electrical faults were located near the breaker (Figure 4(h)), and at the end of the power line sections 28 (Figure 4(i)) and 38 (Figure 4(j)) for the tests. In Figure 4, the results were collected as MATLAB files. IntelliRupters were used in the 12.47 kV Riverside—EPB of Chattanooga utility grid [13]. However, an inverse time overcurrent relay with

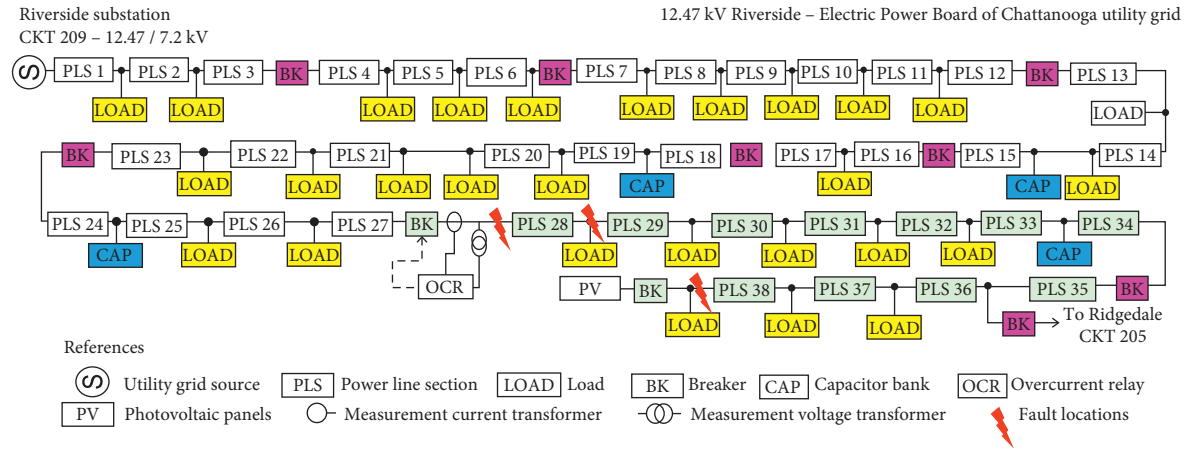

Figure 3: Single-line diagram of 12.47 kV Riverside—EPB of Chattanooga utility grid.

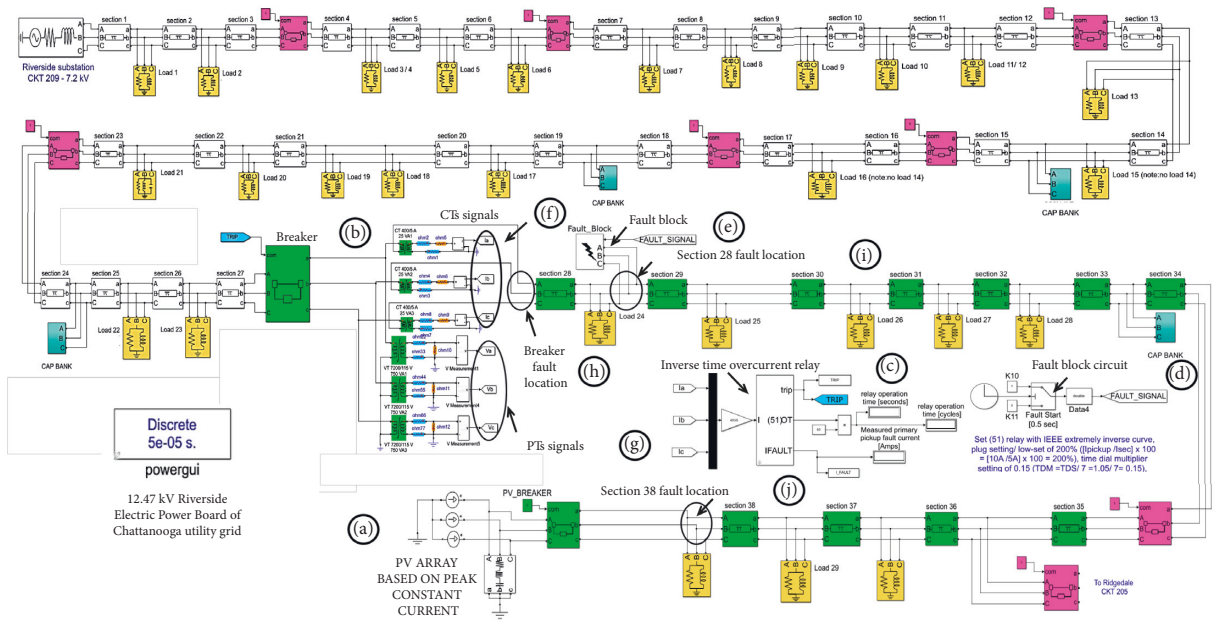

Figure 4: Three-line diagram in MATLAB/Simulink model with (a) power grid circuit, (b) breaker, (c) inverse time overcurrent relay, (d) fault block circuit, (e) fault block, (f) current and (g) potential transformers, and (h–j) fault locations.

saturated measurement transformer models (MATLAB/Simulink) was used on this study. The phase currents and phase to neutral voltages at the breaker location (Figure 4(b)) were collected from the saturated current transformers (CTs) and potential transformers (PTs), which were connected to a cable lead of 1.5 ohms, with relay impedances of 0.0108 ohms for CTs and 240,000 ohms for PTs. The ratios of the CTs and PTs were 400/5 A and 7,200/115 V, respectively.

The inverse time overcurrent relay model (Figure 4(c)) was set with a time dial setting (TDS) of 1.05 s, current transformer ratio (CTR) of 80, relay current pickup (I_P) of 10 amps, and IEEE extremely inverse curve as shown in the following equation.

$$T_R = \frac{TDS}{7} \times \left(0.1217 + \frac{28.2}{\left(I_{\text{primary}}/CTR/I_P \right)^2 - 1} \right) \times 60, \tag{13}$$

where T_R is the relay time in cycles and I_{primary} is the primary current in amps. The inverse time overcurrent relay allowed to open the breaker (Figure 4(b)) at the electrical fault currents. The grid simulation events were run for 3 s to observe the prefault, fault, and post-fault states for each test. The simulated grid test events included the effect of the electrical fault resistance because the fault block (Figure 4(e)) was set with an electrical fault resistance of 0.001 ohms. Table 3 shows the grid simulation tests.

Table 3: Grid simulations tests.

Mode	Electrical fault locations	Type of tests (states)	N° tests (N° states)	Sensors
Grid simulation	Near breaker	AG, BG, CG, AB, BC, AC, ABG, BCG, ACG, ABC, and ABCG electrical faults (prefault, fault, and postfault states)	33 (99)	Saturated CTs/PTs MATLAB/Simulink models
	Power line section 28	AG, BG, CG, AB, BC, AC, ABG, BCG, ACG, ABC, and ABCG electrical faults (prefault, fault, and postfault states)		
	Power line section 38	AG, BG, CG, AB, BC, AC, ABG, BCG, ACG, ABC, and ABCG electrical faults (prefault, fault, and postfault states)		

Table 4: Steps to calculate the phase/ground boundaries of the faulted zones.

1—Calculation of the total resistance and reactance from the power line sections 28 to 38				2—Calculation of the total admittances	3—Calculation of the boundaries
Positive sequence resistance and reactance (equation (14))		Total resistance (equation (5)) and reactance (equation (6))		Total admittance magnitude (equation (7))	Phase-faulted zone boundary (equation (9))
R_{T1}	X_{T1}	$R_T = 2R_{T1} + R_{T0}$	$X_T = 2X_{T1} + X_{T0}$	$\lvert Y_T \rvert$	$\lvert Y_{pg} \rvert > \lvert Y_T \rvert$
0.3044 Ω	**0.3900 Ω**	**1.1518 Ω**	**1.9904 Ω**	**0.435** S	$\lvert Y_{pg} \rvert >$ **0.435 S**
Zero sequence resistance and reactance (equation (15))				Total zero sequence admittance magnitude (equation (8))	Ground faulted zone boundary (equation (10))
R_{T0}	X_{T0}			$\lvert Y_{T0} \rvert$	$\lvert Y_{pg} \rvert > \lvert Y_{T0} \rvert$
0.5430 Ω	**1.2104 Ω**			**0.754 S**	$\lvert Y_{pg} \rvert >$ **0.754 S**

In this study, the proposed method was based on measuring the magnitudes of the PGFA admittance at the faulted phases. Then, the positive, negative, and zero sequence impedances of the power line sections (Figure 4) from the breaker (Figure 4(b)) location to the last feeder were computed. The positive and negative sequence impedances of the power line sections were similar. The total positive sequence (Z_{T1}) and zero sequence (Z_{T0}) impedances in ohms were calculated with equations (14) and (15), respectively, and expressed in standard complex notation with i as the imaginary unit resistance.

$$Z_{T1} = \sum R_{L1} + i \sum X_{L1} = R_{T1} + i X_{T1}, \quad (14)$$

where R_{T1} is the total positive sequence resistance in ohms, X_{T1} is the total positive sequence reactance in ohms, R_{L1} is the positive sequence resistance of each power line section in ohms, and X_{L1} is the positive sequence reactance of each power line section in ohms.

$$Z_{T0} = \sum R_{L0} + i \sum X_{L0} = R_{T0} + iX_{T0}, \quad (15)$$

where R_{T0} is the total zero sequence resistance in ohms, X_{T0} is the total zero sequence reactance in ohms, R_{L0} is the zero sequence resistance of each power line section in ohms, and X_{L0} is the zero sequence reactance of each power line section in ohms.

The steps to calculate the phase/ground boundaries of the PGFA admittance method for the faulted zones are shown in Table 4. The total resistance (R_T) and reactance (X_T), and total zero sequence resistance (R_{T0}) and reactance (X_{T0}) from the power line section 28 to 38 (Figure 4) were calculated. Then, the magnitudes for the total ($|Y_T|$) and total zero sequence ($|Y_{T0}|$) admittances were estimated by equations (7) and (8), respectively, to define the phase and ground faulted zone boundaries for the PGFA admittance method. The boundaries of the PGFA admittance method for the phase and ground faulted zones were $|Y_T| > 0.435$ siemens and $|Y_{T0}| > 0.754$ siemens, respectively.

3.4. Experimental Model. The experimental model was performed with MATLAB/Simulink software and set at the 12.47 kV Riverside—EPB of Chattanooga utility grid (Figure 4). The algorithm model for the PGFA impedance is shown in Figure 5, and it has the sequence impedance setting inputs (Figure 5(a)) and the PGFA impedance algorithm block (Figure 5(b)). From the experimental model, the test mode settings (Figure 6(a)) were selected to run the tests as grid simulation mode or signature library mode, the current/voltage scope (Figure 6(b)) and fault type detection scope (Figure 6(c)) supervised the tests, and the fault type detection logic circuit (Figure 6(d)) identified the types of electrical faults.

In the grid simulation mode, the test mode setting was 0 to start each test (Figure 6(a)), which was run for up to 3 s. Before running the grid simulation tests, the sequence impedances (Figure 6(a)) were set to feed the PGFA impedance algorithm block (Figure 6(b)) and fault type detection logic (Figure 6(d)). The PGFA admittance was calculated with the $1/\pi$ block at the fault type detection scope (Figure 6(c)). The fault block was set with a type of electrical fault (LG, LL, LLG, 3L, or 3LG), and placed near the breaker—or at the end of the power line section 28 or 38 in the power grid circuit (Figure 4)—and the fault block was tripped at 0.5 s.

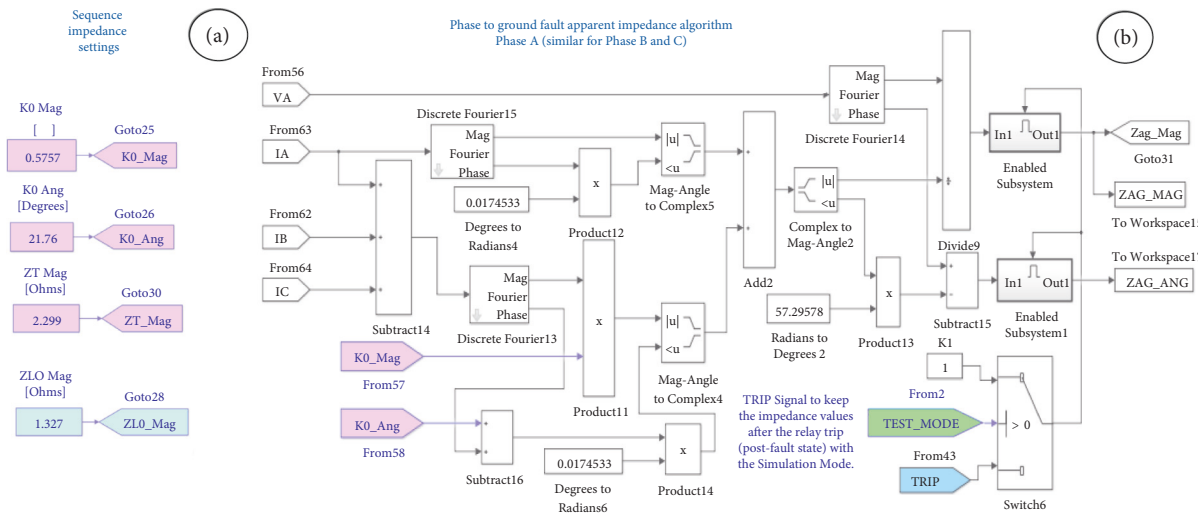

Figure 5: Model with (a) sequence impedance settings and (b) PGFA impedance algorithm block.

and grid simulation tests, the scopes (Figures 6(b) and 6(c))

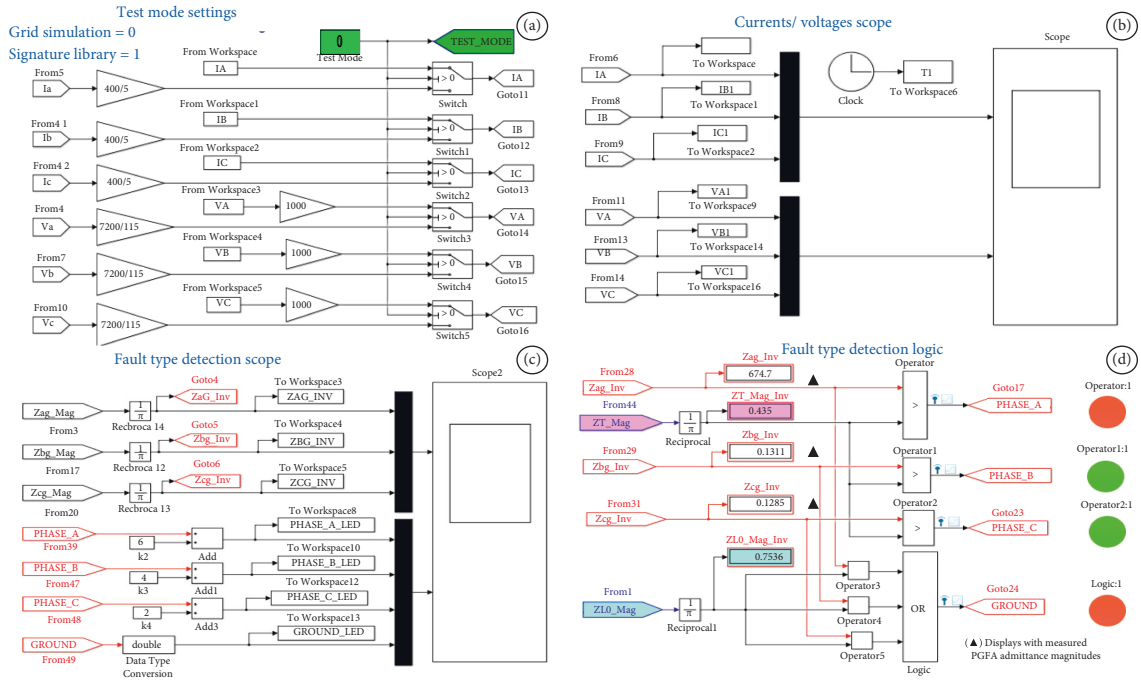

Figure 6: Model with (a) test mode settings, (b) currents/voltages scope, (c) fault type detection scope, and (d) logic circuit.

In the signature library mode, the test mode setting was 1 to start each test (Figure 6(a)) and read the signature library events in the MATLAB workspace. Furthermore, the signature library tests were run by downloading a signature library event in the MATLAB workspace. This signature library consists of multiple real data sets, phase currents, and voltages collected from the optical power line sensors deployed on the field, at the 46 kV EPB of Chattanooga electrical substation. Once the simulation was running, the phase currents and voltages were measured, and the PGFA admittances were calculated and observed in the scopes (Figures 6(b) and 6(c)). For the signature library were used to supervise the simulations. After running the signature library and grid simulation tests, the output signals were saved in the MATLAB workspace to plot and analyze the data collected. In the grid simulation tests, the overcurrent relay trip signal (Figure 4(c)) at the fault state kept the measured PGFA admittance magnitudes and angles after the fault state. Then, the relays kept the sates of LEDs for the type of electrical fault during the postfault states to observe the nature of faults. However, in the signature library tests, the overcurrent relay did not trip because the tests were based on reading the currents and voltages from the stored events.

Table 5: Measured PGFA admittance and impedance magnitudes of the fault states.

Test names: test mode-fault location-type of fault	Groups	PGFA admittance and impedance magnitudes			Figure 7
		Phase A Siemens (ohms)	Phase B Siemens (ohms)	Phase C Siemens (ohms)	
Grid-simulation-breaker-AG fault		**674.7** (0.0015)			
Grid-simulation-breaker-BG fault	LG-BK		**675.2** (0.0015)		
Grid-simulation-breaker-CG fault				**675.2** (0.0015)	
Grid-simulation-breaker-ABG fault		**810.2** (0.0012)	**670.1** (0.0015)		
Grid-simulation-breaker-BCG fault	LLG-BK		**811.5** (0.0012)	**670.5** (0.0015)	
Grid-simulation-breaker-ACG fault		**670.4** (0.0015)		**811.9** (0.0012)	
Grid-simulation-breaker-AB fault		**0.7125** (1.4035)	**0.7046** (1.4192)		
Grid-simulation-breaker-BC fault	LL-BK		**0.713** (1.4025)	**0.7053** (1.4178)	
Grid-simulation-breaker-AC fault		**0.7046** (1.4192)		**0.7125** (1.4035)	
Grid-simulation-breaker-ABCG fault	3LG-BK	**786.8** (0.0013)	**786.9** (0.0013)	**786.9** (0.0013)	
Grid-simulation-breaker-AB fault	3L-BK	**786.8** (0.0013)	**786.9** (0.0013)	**786.9** (0.0013)	
Grid-simulation-section-28-AG fault		**22.91** (0.0436)			
Grid-simulation-section-28-BG fault	LG-28		**22.93** (0.00436)		
Grid-simulation-section-28-CG fault				**22.93** (0.00436)	
Grid-simulation-section-28-ABG fault		**21.48** (0.0466)	**22.26** (0.0449)		
Grid-simulation-section-28-BCG fault	LLG-28		**21.54** (0.0464)	**22.28** (0.0449)	
Grid-simulation-section-28-ACG fault		**22.29** (0.0449)		**21.58** (0.0463)	
Grid-simulation-section-28-AB fault		**0.6910** (1.4472)	**0.7022** (1.4241)		
Grid-simulation-section-28-BC fault	LL-28		**0.6915** (1.4461)	**0.7027** (1.4231)	
Grid-simulation-section-28-AC fault		**0.7022** (1.4241)		**0.6910** (1.4472)	
Grid-simulation-section-28-ABCG fault	3LG-28	**20.84** (0.0480)	**20.85** (0.0480)	**20.85** (0.0480)	
Grid-simulation-section-28-AB fault	3L-28	**20.84** (0.0480)	**20.85** (0.0480)	**20.85** (0.0480)	
Grid-simulation-section-38-AG fault		**1.974** (0.5066)			
Grid-simulation-section-38-BG fault	LG-38		**1.974** (0.5066)		
Grid-simulation-section-38-CG fault				**1.974** (0.5066)	
Grid-simulation-section-38-ABG fault		**1.974** (0.5066)	**1.990** (0.5025)		
Grid-simulation-section-38-BCG fault	LLG-38		**1.975** (0.5063)	**1.991** (0.5023)	
Grid-simulation-section-38-ACG fault		**1.991** (0.5023)		**1.976** (0.5061)	
Grid-simulation-section-38-AB fault		**0.5426** (1.843)	**0.5951** (1.6804)		
Grid-simulation-section-38-BC fault	LL-38		**0.5426** (1.8430)	**0.5951** (1.6804)	
Grid-simulation-section-38-AC fault		**0.5951** (1.6804)		**0.5426** (1.8430)	
Grid-simulation-section-38-ABCG fault	3LG-38	**1.988** (0.5030)	**1.987** (0.5033)	**1.990** (0.5025)	
Grid-simulation-section-38-ABC fault	3L-38	**1.988** (0.5030)	**1.987** (0.5033)	**1.990** (0.5025)	
Signature-library-SIGID-934 (optical power line sensors)	LG-934		**0.270** (3.7037)		

4. Results

4.1. Fault States. The measured PGFA admittance magnitudes for the fault states of the grid simulation and signature library events were computed to assess the types of electrical faults. The measured PGFA admittance and impedance magnitudes for the A, B, and C phases at the fault states are shown in Table 5. The test events were grouped into the types of electrical faults and their locations. The measured PGFA impedance and admittance magnitudes from Table 5 were plotted in Figure 7. Therefore, the measured PGFA impedance and admittance magnitudes are represented in the vertical (decimal scale) and horizontal (logarithmic scale) axes, respectively. The black curve means the expected path of the measured PGFA admittance magnitudes. The pink ($|Y_T|$) and blue ($|Y_{T0}|$) dotted lines are the phase and ground boundaries, respectively, based on the $|Y_T|$ and $|Y_{T0}|$ numerical values from Table 4. For the grid simulation tests, the LG, LLG, LL, 3LG, and 3L electrical faults near the breaker and at the end of the power line sections 28 and 38 were set at the faulted zone in Figure 7. The measured PGFA admittance magnitudes for the LG, LLG, 3LG, and 3L electrical faults were greater than 0.754 siemens. However, the measured PGFA admittance magnitudes for the LL electrical faults were set between 0.754 and 0.435 siemens. Therefore, the LLG and LL electrical faults were distinguished satisfactorily because both types of electrical faults generated different measured PGFA admittance magnitudes. However, the 3LG and 3L electrical faults generated similar measured PGFA admittance magnitudes.

4.2. Confusion Matrix and Results. The PGFA admittance method with phase/ground boundaries was evaluated with the confusion matrix [27, 28]. In this matrix, the matching between the predicted (expected) and measured (observed) values for all tests were compared. In the PGFA admittance model (Figure 8), the model inputs and outputs are presented.. The model inputs were the expected values (known data) stated by the phase currents

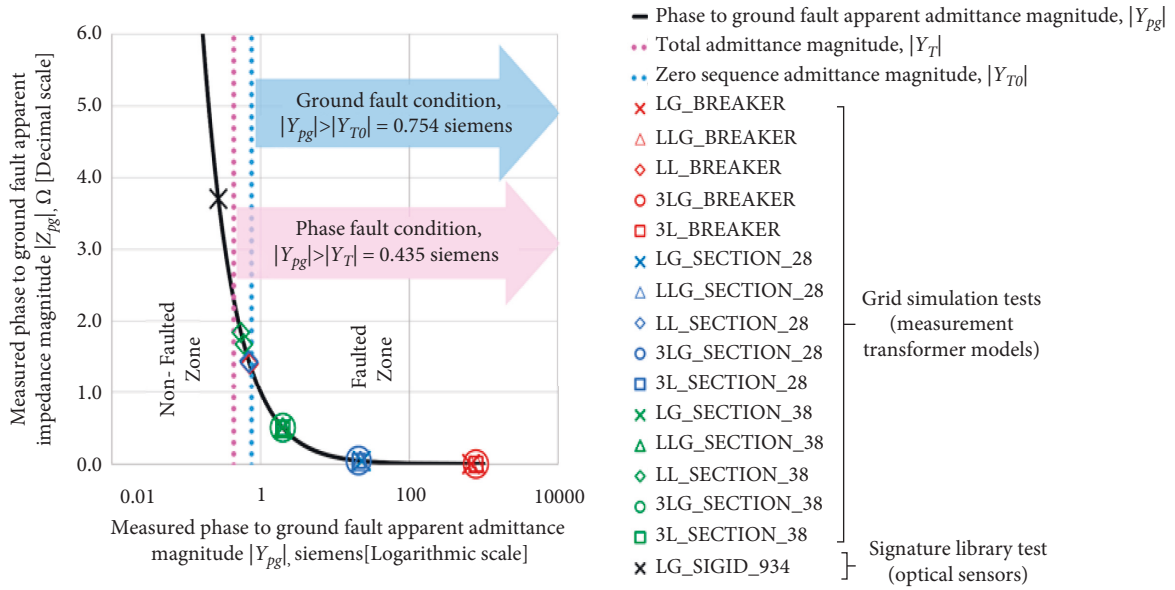

Figure 7: Measured PGFA admittance magnitudes for the fault states.

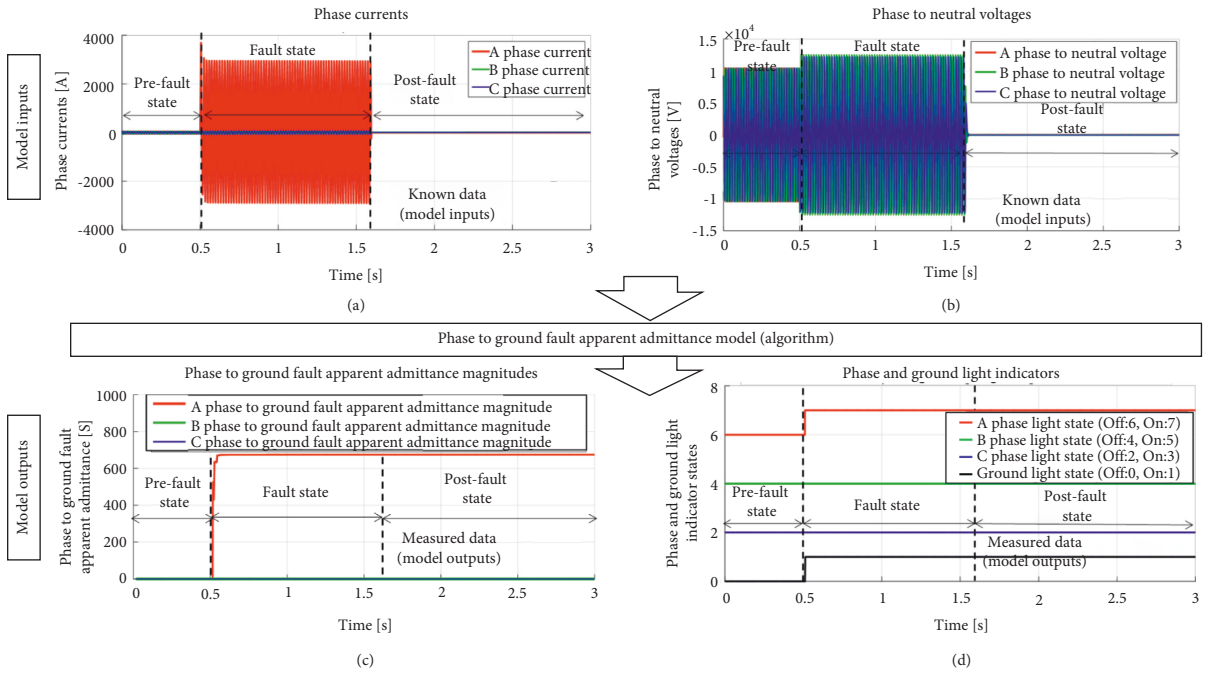

Figure 8: PGFA admittance model (a, b) inputs and (c, d) outputs.

(Figure 8(a)) and voltages (Figure 8(b)) at the nonfaulted (prefault state) and faulted (fault state) situations. The model outputs were the observed values (measured data) stated by the PGFA admittance magnitudes (Figure 8(c)), and the A, B, and C phase/ground LEDs (Figure 8(d)) at the nonfaulted (prefault state) and faulted (fault sate) situations.

Table 6 shows the predicted values and measured true positive (*TP*), false positive (*FP*), true negative (*TN*), and false negative (*FN*) values from the tests. The *TP* and *FN* values were considered when the fault-predicted values matched and did not match the measured values, respectively. The *TN* and *FP* values were considered when the non-fault-predicted values matched and did not match the measured values, respectively. The confusion matrix for the PGFA admittance method was created based on using the 105 measured values from Table 6. The measured *TP*, *FP*, *TN*, and *FN* values were 64, 0, 35, and 6, respectively. The measured *TP*, *FP*, *TN*, and *FN* values in percent were calculated for the 105 sets, and the results are shown in Figure 9.

The results from the confusion matrix (*TP*, *FP*, *TN*, and *FN* values) were used to calculate the class statistics values such as the accuracy (Accuracy (%)), precision (Precision

Table 6: Predicted values and measured *TP*, *FP*, *TN*, and *FN* values.

Tests names: test mode-fault location-type of fault	Predicted values	Number of measured values			
		TP	*FP*	*TN*	*FN*
Grid-simulation-breaker-AG fault Grid-simulation-breaker-BG fault Grid-simulation-breaker-CG fault Grid-simulation-section-28-AG fault Grid-simulation-section-28-BG fault Grid-simulation-section-28-CG fault Grid-simulation-section-38-AG fault Grid-simulation-section-38-BG fault Grid-simulation-section-38-CG fault	PRFS, FS, POFS	$9^{(FS)}$, $9^{(POFS)}$		$9^{(PRFS)}$	
Grid-simulation-breaker-ABG fault Grid-simulation-breaker-BCG fault Grid-simulation-breaker-ACG fault Grid-simulation-section-28-ABG fault Grid-simulation-section-28-BCG fault Grid-simulation-section-28-ACG fault Grid-simulation-section-38-ABG fault Grid-simulation-section-38-BCG fault Grid-simulation-section-38-ACG fault	PRFS, FS, POFS	$9^{(FS)}$, $9^{(POFS)}$		$9^{(PRFS)}$	
Grid-simulation-breaker-AB fault Grid-simulation-breaker-BC fault Grid-simulation-breaker-AC fault Grid-simulation-section-28-AB fault Grid-simulation-section-28-BC fault Grid-simulation-section-28-AC fault Grid-simulation-section-38-AB fault Grid-simulation-section-38-BC fault Grid-simulation-section-38-AC fault	PRFS, FS, POFS	$9^{(FS)}$, $9^{(POFS)}$		$9^{(PRFS)}$	
Grid-simulation-breaker-ABCG fault Grid-simulation-section-28-ABCG fault Grid-simulation-section-38-ABCG fault	PRFS, FS, POFS	$3^{(FS)}$, $3^{(POFS)}$		$3^{(PRFS)}$	
Grid-simulation-breaker-ABC fault Grid-simulation-section-28-ABC fault Grid-simulation-section-38-ABC fault	PRFS, FS, POFS			$3^{(PRFS)}$	$3^{(FS)}$, $3^{(POFS)}$
Signature-library-SIGID-931	NFS			$1^{(NFS)}$	
Signature-library-SIGID-932	POFS	$1^{(POFS)}$			
Signature-library-SIGID-933	POFS	$1^{(POFS)}$			
Signature-library-SIGID-934	PRFS, FS, POFS	$1^{(FS)}$, $1^{(POFS)}$		$1^{(PRFS)}$	
Measured *TP*, *FP*, and *TN* values $(64+0+35+6=105)$ (%)		64 (61%)	0 (0%)	35 (33.3%)	6 (5.7%)

Predicted values: prefault state (PRFS), fault state (FS), postfault state (POFS), and nonfault state (NFS).

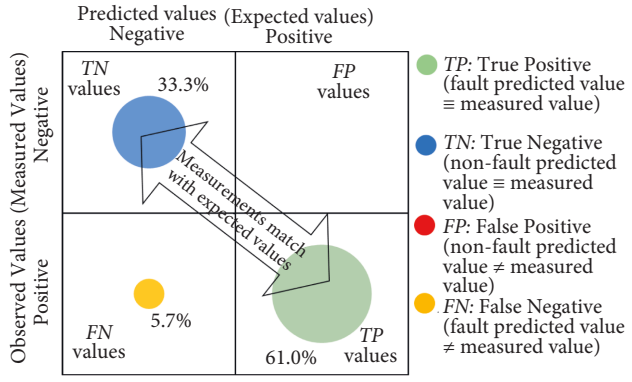

Figure 9: Confusion matrix for the PGFA admittance method.

(%)), sensitivity (Sensitivity (%)), specificity (Specificity (%)) and error rate (Error rate (%)) to quantify the model performance [27, 28]. The Accuracy (%) is the degree of closeness to the true value, and it is calculated by the following equation:

$$\text{Accuracy}_{\%} = \left[\frac{TP + TN}{(TP + FP + TN + FN)}\right] \times 100. \tag{16}$$

The Precision (%) is the degree to which a process will repeat the same value, such as when a positive event is predicted and how often it is correct; it is calculated by the following equation:

Table 7: Accuracy, precision, sensitivity, specificity, and error rate.

Accuracy (%) equation (16)	Precision (%) equation (17)	Sensitivity (%) equation (18)	Specificity (%) equation (19)	Error rate (%) equation (20)
94.3%	100%	91.4%	100%	5.7%

$$\text{Precision}_{\%} = \left[\frac{TP}{FP + TP}\right] \times 100. \quad (17)$$

The Sensitivity (%) measures the true positive rate, when it is a positive event, and how often it is predicted as positive; it is given by the following equation.

$$\text{Sensitivity}_{\%} = \left[\frac{TP}{TP + FN}\right] \times 100. \quad (18)$$

The Specificity (%) measures the true negative rate, when it is a negative event, and how often it is predicted as negative; it can be computed by the following equation.

$$\text{Specificity}_{\%} = \left[\frac{TN}{TN + FP}\right] \times 100. \quad (19)$$

The Error rate (%) measures how often the measured values are wrong, and it is calculated by the following equation.

$$\begin{aligned}\text{Error rate}_{\%} &= 100 - \text{Accuracy}_{\%} \\ &= \left[1 - \frac{TP + TN}{(TP + FP + TN + FN)}\right] \times 100.\end{aligned} \quad (20)$$

Table 7 shows the class statistics values of the PGFA admittance model, based on calculating the Accuracy (%), Precision (%), Sensitivity (%), Specificity (%), and Error rate (%) with the measured *TP*, *FP*, *TN*, and *FN* values from the test results in Table 6.

The Accuracy (%) of the PGFA admittance method was 94.3% because it did not distinguish between the 3L and 3LG electrical faults. The Precision (%) of the PGFA admittance method was 100% because when the predicted values were faulted, the measured values were faulted, and when the predicted values were nonfaulted, the measured values were nonfaulted. The Sensitivity (%) was 91.4% because the postfault and fault states for the 3L electrical faults of the simulated grid events were *FN* values instead of *TP* values (Table 6). The Specificity (%) was 100% because the nonfault and prefault states for all test events were always *TN* values (Table 6), and the Error rate (%) was 5.7%.

5. Discussion

In the signature library mode, the COMTRADE events were converted into MATLAB files. The measured phase currents and voltages (26.6 kV phase-to-ground voltage) from the optical power line sensors deployed on the field at the 46 kV EPB of Chattanooga electrical substation were represented by the events shown in Table 2. The SIGID-931, SIGID-932, and SIGID-934 events were plotted in this section.

The SIGID-931 event was a service restoring of the A, B, and C phase feeders (nonfault state). Figure 10 shows the currents, voltages, PGFA admittance magnitudes, and PGFA conductance/susceptance from the optical power line sensors deployed on the field. When the service was restored, the currents increased considerably (Figure 10(a)), and the voltages were similar to the pre-restoring service state (Figure 10(b)). However, the PGFA admittance magnitudes increased from 0 to 0.009 siemens (Figure 10(c)). Consequently, the dynamic paths of the PGFA admittances before and after restoring the service were practically at the same location, moving from a conductance of 0 to −0.007 siemens (Figure 10(d)). The SIGID-931 event was a nonfault situation because the PGFA admittance magnitudes for the states before and after restoring the service (Figure 10(c)) were too small to detect the types of electrical faults.

The SIGID-932 event was a phase C to ground electrical fault that blown a fuse (postfault state). Figure 11 shows the currents, voltages, PGFA admittance magnitudes, and PGFA conductance/susceptance from the optical power line sensors deployed on the field. This event shows the postfault state when the phase C fuse was melted, and the measured current (Figure 11(a)) and voltage (Figure 11(b)) of the phase C were near zero. However, the measured PGFA admittance magnitude of the phase C was greater than zero (Figure 11(c)), observing the detection of phase C to ground electrical fault at the postfault state. Consequently, the dynamic path of the PGFA admittance for the phase C was represented by a circle with a radius of approximately 2 siemens, and the PGFA admittances of phase A and B were practically zero (Figure 11(d)).

The SIGID-934 event was a phase B to ground electrical fault. Figure 12 shows the currents, voltages, PGFA admittance magnitudes, and PGFA conductance/susceptance from the optical power line sensors deployed on the field. The SIGID-934 event was stated by the prefault, fault, and postfault states. At the fault state, the measured phase B current increased (Figure 12(a)), and the phase B to ground voltage decreased (Figure 12(b)). This event could be a temporary phase B to ground electrical fault. The measured PGFA admittance magnitude of the phase B increased more than the other phases (Figure 12(c)). Consequently, the dynamic path of the PGFA admittance for the phase B was greater than for the phase A and C (Figure 12(d)).

In the simulation grid mode, the currents and voltages from the saturated measurement transformer models were simulated at the 12.47 kV Riverside—EPB of Chattanooga utility grid (Figure 4). Figure 13 shows the measured PGFA admittance magnitudes for the AB and ABG electrical faults near the breaker and at the end of the power line section 38. The dynamic responses of the measured PGFA admittance magnitudes at the AB electrical faults near the breaker

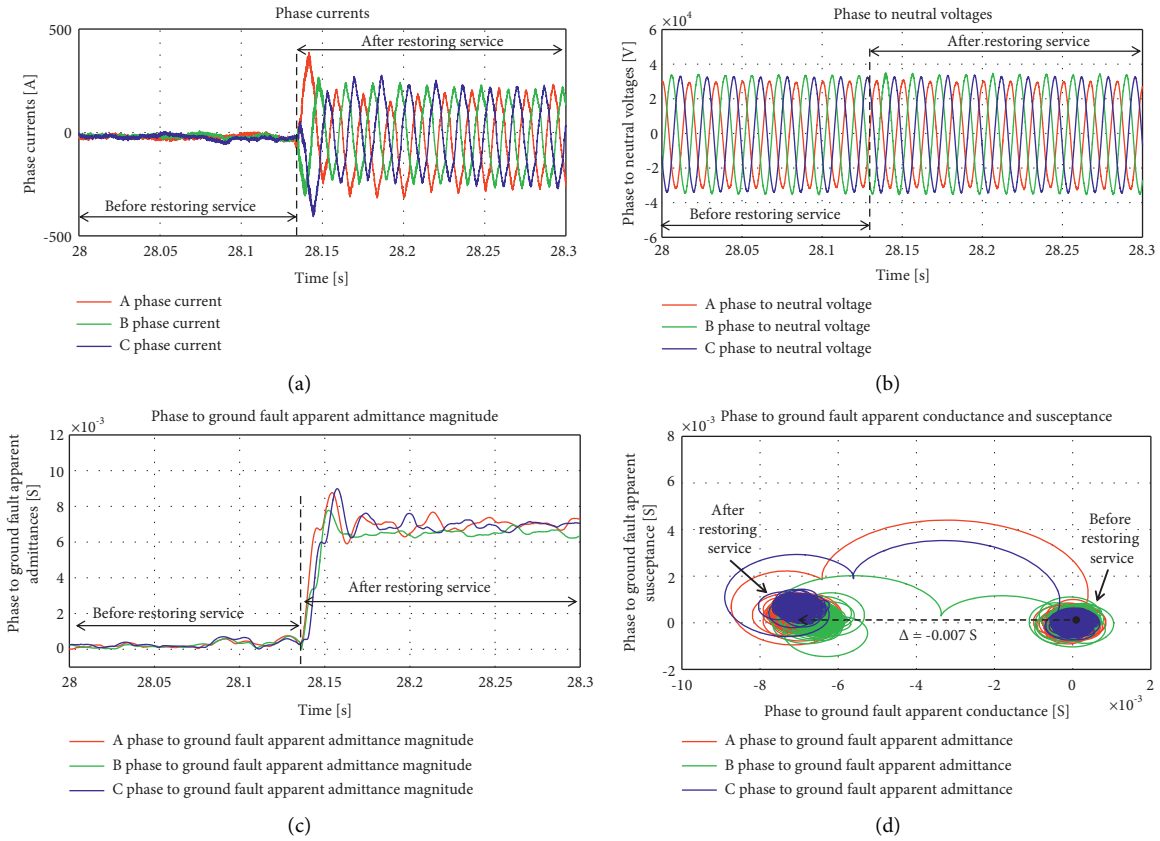

Figure 10: SIGID-931 event (a) currents, (b) voltages, (c) PGFA admittance magnitudes, and (d) PGFA conductance/susceptance from the optical power line sensors deployed on the field.

(Figure 13(a)) and at the end of the power line section 38 (Figure 13(c)) were detected as nongrounding faults because the faulted phases were between 0.435 siemens ($|Y_T|$) and 0.754 siemens ($|Y_{T0}|$). However, the dynamic responses of the measured PGFA admittance magnitudes at the ABG electrical faults near the breaker (Figure 13(b)) and at the end of power line section 38 (Figure 13(d)) were detected as grounding faults because the faulted phases were greater than 0.754 siemens ($|Y_{T0}|$). Figure 14 shows the measured PGFA admittance magnitudes for the AG and ABCG/ABC electrical faults at the end of power line sections 28 and 38. The dynamic responses of the measured PGFA admittance magnitudes at the AG and ABCG electrical faults at the end of the power line sections 28 (Figures 14(a) and 14(b)) and 38 (Figures 14(c) and 14(d)) were detected satisfactorily as grounding electrical faults because the faulted phases were greater than 0.754 siemens ($|Y_{T0}|$). However, the dynamic response of the measured PGFA admittance magnitudes at the ABCG and ABC electrical faults was similar, without distinguishing between these electrical faults.

The examination of the PGFA admittance method with phase/ground boundaries was performed by using the signature library events and grid simulations. In the simulated grid events, the test results were collected from the saturated measurement transformers connected to a radial power system that was connected to a three-phase voltage source connected in Wye to an internally grounded neutral (7.2 kV phase to neutral voltage), at the 12.47 kV Riverside—EPB of Chattanooga utility grid (Figure 4). However, in the signature library events, the test results were collected from the optical power line sensors (26.6 kV phase to neutral voltage) deployed on the field, at the 46 kV EPB of Chattanooga electrical substation with delta-wye power transformers (insulated neutral point), that do not allow to pass the zero sequence. However, the phase B to ground electrical fault event (SIGID-934) from the optical power line sensors (Figures 12(c) and 12(d)) had shown a good behavior by measuring the highest admittance magnitudes at the faulted phase.

In this study, the PGFA admittance method with phase/ground boundaries could not differentiate between the 3LG and 3L electrical faults; however, it could differentiate between the LG, LL, and LLG electrical faults. However, the sequence method [3] that detects the types of electrical faults by measuring the angle between the negative and zero sequence currents [3], the AG/BCG, CG/ABG, and BG/CAG electrical faults had the same detection conditions [3]. Therefore, the PGFA admittance method with phase/ground boundaries could perform better than the sequence method, considering the LG/LLG electrical faults are more frequent than the 3LG/3L electrical faults in power grids. However, the sequence method has the advantage that it did not require additional settings [3, 4].

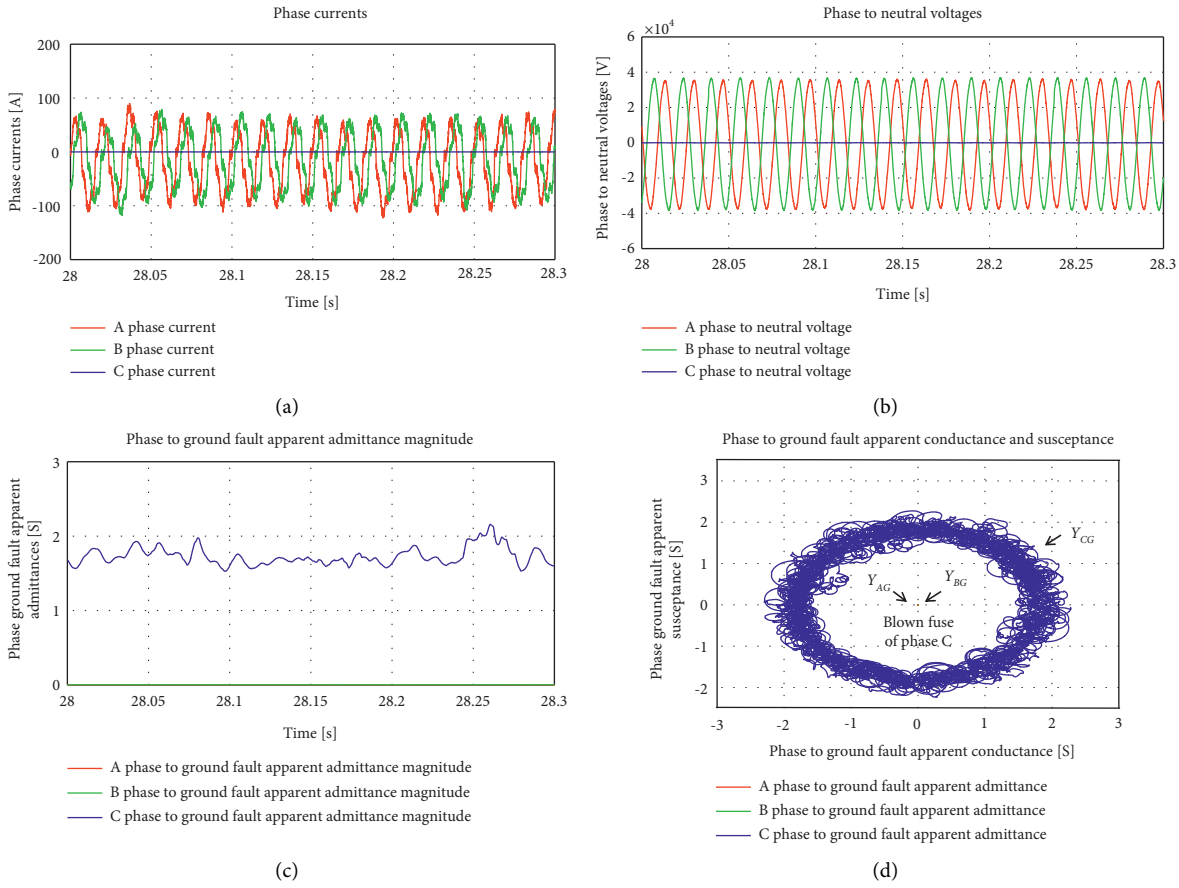

Figure 11: SIGID-932 event (a) currents, (b) voltages, (c) PGFA admittance magnitudes, and (d) PGFA conductance/susceptance from the optical power line sensors deployed on the field.

In the computational process of generating or measuring transient events with high-frequency components at electrical faults, protection algorithms and power system simulations need to process the phase current and voltage signals with small time steps. This computational process depends on the sampling frequency related to the Nyquist sampling theorem [29], and the sampling frequency of a signal should be at least twice the bandwidth of the signal to avoid aliasing. Then, the Nyquist theorem can be written by the following equation:

$$F_{\text{sampling}} \geq 2F_{\text{max}}, \tag{21}$$

where F_{sampling} is the sampling frequency in (Hz), and F_{max} is the largest frequency component of the signal in (Hz). From equation (21), the lowest frequency is assumed to be 0 Hz, and the aliasing happens when signals are sampled at sub-Nyquist rate ($F_{\text{sampling}} < 2\ F_{\text{max}}$). Also, the time step and samples per cycle of measured signals can be estimated by following equations (22) and (23), respectively.

$$T_{\text{step}} = \frac{1}{F_{\text{sampling}}} \times 10^6, \tag{22}$$

$$S_{\text{cycle}} = \frac{F_{\text{sampling}}}{60}, \tag{23}$$

where T_{step} is the time step in microseconds, F_{sampling} is the sampling frequency in Hz, and S_{cycle} is the samples per cycle for a 60 Hz signal.

The protection algorithm for the PGFA admittance method with phase/ground boundaries was performed in a MATLAB/Simulink model, using simulations with a time step of 50 microseconds for the simulated grid events, at the 12.47 kV Riverside—EPB of Chattanooga utility grid. However, in the signature library events (SIGID-931, SIGID-932, SIGID-933, and SIGID-934) for the optical power line sensor deployed on the field at the 46 kV EPB of Chattanooga electrical substation, the sampling frequency of the events was 20,000 Hz that represents 333.33 samples per cycle, based on equation (23), and a time step of 50 microseconds, based on Equation (22). It shows the important role of the sampling frequency in the computational burden process for the PGFA admittance method with phase/ground boundaries.

In this study, the CT and PT saturated measurement transformer models [25] were performed in the MATLAB/Simulink software for the PGFA admittance model and the 12.47 kV Riverside—EPB of Chattanooga utility grid. Then, the measured phase current and voltage signals injected to the PGFA admittance model considered the CT/PT saturation effect. The PGFA admittance algorithm was based on using an inverse distance protection element that can be

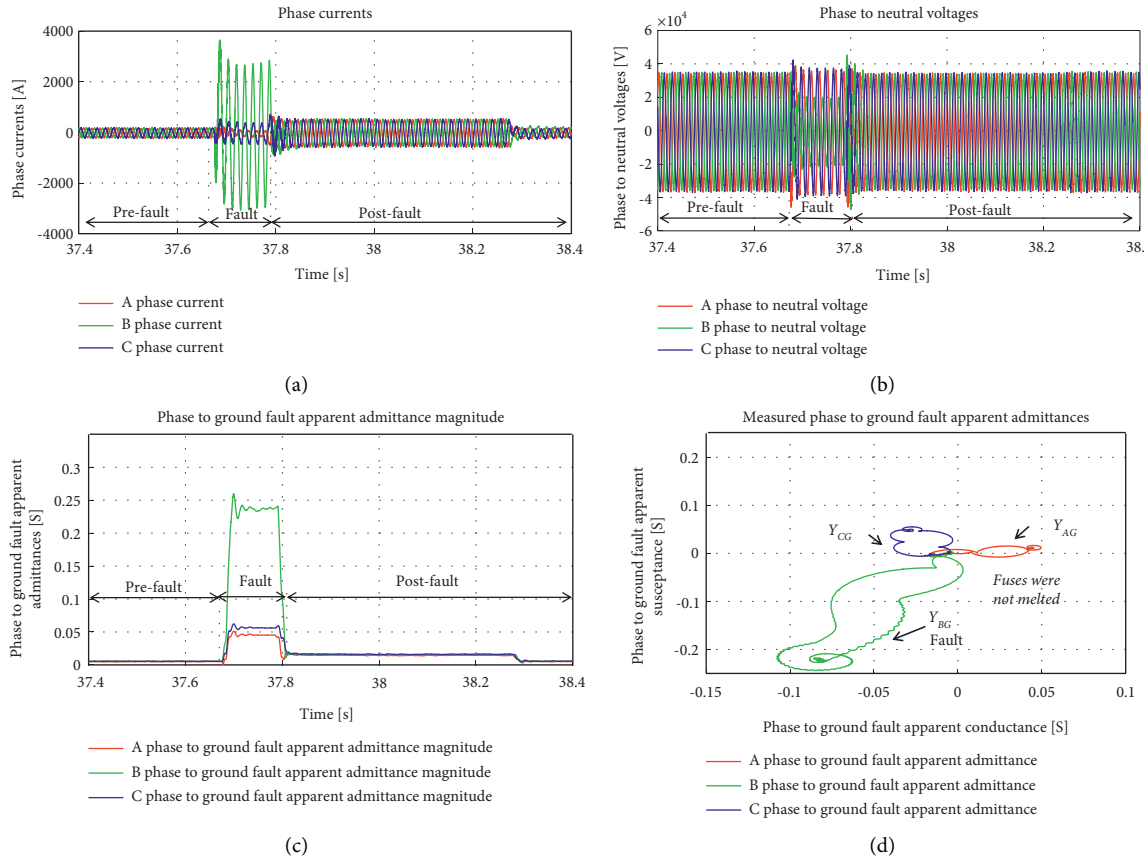

FIGURE 12: SIGID-934 event (a) currents, (b) voltages, (c) PGFA admittance magnitudes, and (d) PGFA conductance/susceptance from the optical power line sensors deployed on the field.

represented by the measurement of a complex current/voltage ratio [30]. Then, the impact of the current/voltage ratio error on the admittance accuracy is represented by the following equation:

$$|Y| = \frac{|I|}{|V|} \longrightarrow \text{Error}_{\%|Y|} = \text{Error}_{\%|I|} - \text{Error}_{\%|V|}, \tag{24}$$

where Y is the measured admittance in siemens, I is the measured current in amps, V is the measured voltage in volts, $\text{Error}_{\%|Y|}$ is the percentage admittance error in percent, $\text{Error}_{\%|I|}$ is the percentage current error in percent, and $\text{Error}_{\%|V|}$ is the percentage voltage error in percent.

From equation (24), if the percent current and voltage errors have the same sign, the percent voltage and current errors are mutually canceled in the ratio. However, the worst-case scenario is when the percent current and voltage errors are of opposite signs. In addition, the measured admittance on transient states with the inverse of the distance protection elements depends on the loop for the measured voltages and currents based on the equivalent circuit defined for the type of electrical faults [30]. That was also considered in the assessment of the PGFA admittance method, by considering different types of electrical faults (LG, LLG, LL, 3L, and 3LG) located at the power line sections during the tests.

In the assessment of the PGFA admittance algorithm, the effect of the fault resistance was considered by using a fault block model from MATLAB/Simulink. The fault and ground resistances were set at 0.001 ohms for the fault block at the simulated grid events of the 12.47 kV Riverside—EPB of Chattanooga utility grid (Figure 4). However, in the signature library events (Table 2), the B phase-to-ground fault event (SIGID-934) included the effect of the fault ground resistance (Figure 12) because it was collected on the field from the current/voltage optical power line sensors at the 46 kV EPB utility substation of Chattanooga. The effect of the load switching was represented by the service restoration of the A, B, and C phase feeders, given by the SIGID-931 event that represented a nonfault state situation (Figure 10). The SIGID-931 event was collected in the field too. After running the SIGID-931 event test with the PGFA admittance algorithm, the A, B, and C phase admittance magnitudes were observed during the restoration of service. Then, the PGFA admittances before and after restoring the service were from 0 to 0.008 siemens (Figure 10(c)), and consequently, the conductance moved from 0 to −0.007 siemens (Figure 10(d)). Therefore, the restoration of service that represents a load switching in the SIGID-931 event was a nonfault situation because the PGFA admittance magnitudes for the states before and after restoring the service (Figure 10(c)) were too small. The effect of the fault inception angles is another aspect to be discussed. Based on the fault, the inception time is the moment at which the

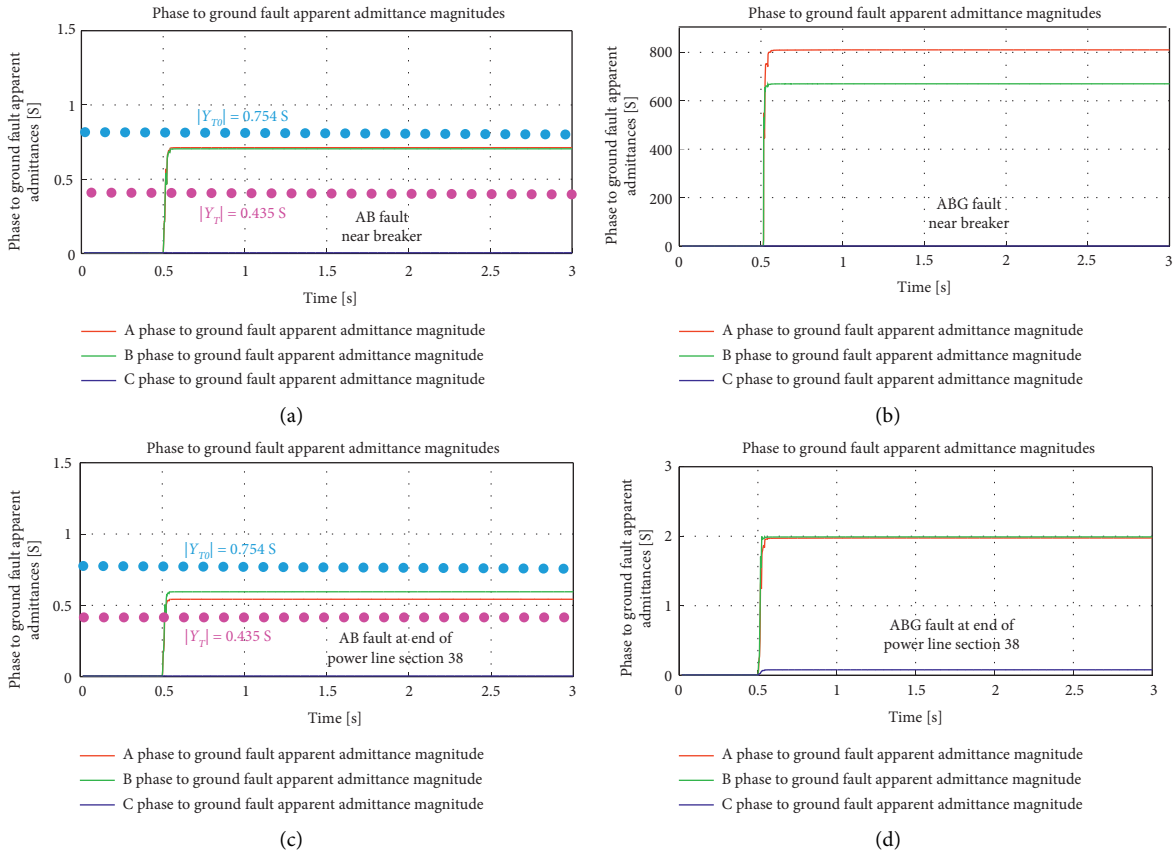

Figure 13: Measured PGFA admittance magnitudes for the grid simulated AB and ABG electrical faults (a, b) near breaker and (c, d) end of the power line section 38 with the CT/PT saturated models.

electrical fault is initiated. The fault inception angle is defined by the voltage phasor (angle) at a ground electrical fault is initiated. The fault inception angle can be changed by varying the time when the electrical fault is initiated. Then, the fault inception angles can generate different transient events for the phase voltage or current signals [31], and consequently also different transient events for the measured PGFA admittances of phases A, B, and C.

The most important methods for detecting the types of electrical faults are based on the state of the art, because they are focused on several innovations applied on measuring impedances [4] and sequence currents at the relay locations [3]. The computationally efficient distance relay for power transmission lines [15] method measures the impedance of the electrical fault loops for multiple zones of distance protection elements, and it depends on a presetting condition for the relay. In another technique, the electrical fault identification system for use in protective relays for power transmission lines [16] method measures the angle between the negative and zero sequence currents, and it is based on an electrical fault identification selection logic that allows to select the types of electrical faults without a presetting condition for the relay, but it addresses the concern that the ground distance elements do not overreach for the LLG electrical faults [16]. In this study, the PGFA admittance method with phase/ground boundaries was presented. It is based on measuring the A, B, and C phase admittance magnitudes for the faulted and nonfaulted phases, resulting in greater than zero and near zero, respectively, and using the phase/ground boundaries to distinguish between the LL and LLG electrical faults. The PGFA admittance method with phase/ground boundaries was based on the computation of the presetting algorithm values by using the zero, positive, and negative sequences of power line sections, to determine the phase and ground boundaries. Table 8 shows the comparison of the methods to detect the types of electrical faults.

In the PGFA admittance method with phase/ground boundaries, the protective relay was set at a specific location along the power line. However, this method could be executed at different protective relay locations along the power line once the presetting conditions were stated. Based on the "Data collection" step from Figure 1, the PGFA admittance method has a relay presetting condition that needs to be calculated by using the total zero (Z_{T0}), positive (Z_{T1}), and negative (Z_{T2}) sequence impedance of the power line sections at the protective relay location. In addition, the PGFA admittance method needs to define the phase ($|Y_T|$) and ground ($|Y_{T0}|$) boundaries from equations (7) and (8), respectively, that depend on the total resistance (R_T), total reactance (X_T), total zero sequence resistance (R_{T0}), and total zero sequence reactance (X_{T0}) of power line sections at the protective relay location. Therefore, the PGFA admittance method with phase/ground boundaries could be performed

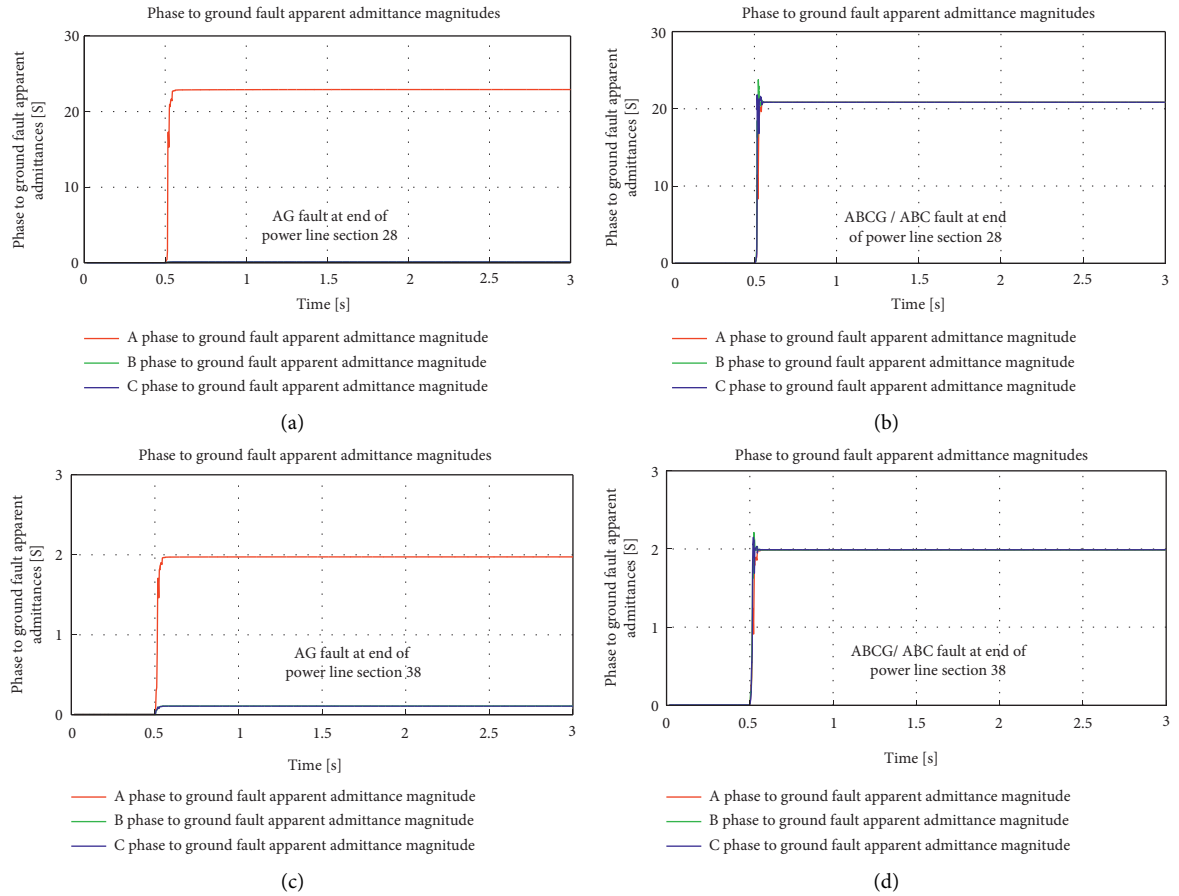

Figure 14: Measured PGFA admittance magnitudes for the grid simulated AG and ABCG/ABC electrical faults at end of the power line section (a, b) 28 and (c, d) 38 with CT/PT saturated models.

Table 8: Comparison of the methods to detect the types of electrical faults.

Methods	Algorithms	Measurement (units)	Relay pre-settings
Computationally efficient distance relay for power transmission lines [4, 15].	This method allows all six impedance loops (AB, BC, CA, AG, BG, and CG) for multiple zones of distance protection elements to be measured and compared every 1/8 cycle [4, 15].	Impedances (Ω)	Yes
Electrical fault finding for protective relays in power transmission lines [4, 16].	This method measures the angle between the negative and zero sequence currents [4, 16].	Angles (°)	No
PGFA admittances with phase/ground boundaries for power lines.	This method measures the A, B, and C phase admittance magnitudes for the faulted and nonfaulted phases, resulting in greater than zero and near zero, respectively.	Admittances (S)	Yes

at different protective relay locations along the power line once the relay presetting conditions were calculated.

As future work, the implementation of the PGFA admittance algorithm on the field based on writing its logic program inside of a protective relay will be performed. Then, the A, B, and C phase and ground outputs from the PGFA admittance algorithm will be set in the target LEDs that indicate the type of electrical faults in the protective relay's front panel. In addition, the PGFA admittance method with phase/ground boundaries will be compared with the protective relay manufacturer method, by using a real-time simulator and two protective relays in the loop.

6. Conclusions

The PGFA admittance method with phase/ground boundaries was evaluated satisfactorily in this study. The faulted phases were detected for the LG, LL, LLG, 3LG, and 3L electrical faults at different bus locations. In addition, the PGFA admittance algorithm was tested with grid simulations (MATLAB/Simulink saturated measurement transformer models) at the 12.47 kV Riverside—EPB of Chattanooga utility grid and signature library events (optical power line sensor deployed on the field) from the 46 kV EPB of Chattanooga electrical substation.

The PGFA admittance method with phase/ground boundaries had shown a good behavior, resulting that the measured PGFA admittance magnitudes were greater than zero and near zero for the faulted and nonfaulted phases, respectively. Whereas the AG/BCG, CG/ABG, and BG/CAG electrical faults had the same detection conditions for the sequence method [3], the PGFA admittance method with phase/ground boundaries could differentiate between the LG and LLG electrical faults, but the PGFA admittance algorithm needed of the calculation of the presetting conditions, to determine the phase and ground boundaries.

The PGFA method with phase/ground boundaries was evaluated with the confusion matrix. The measured and predicted values (faulted and nonfaulted phases) matched in more than 90% of the tests, and the PGFA admittance method with phase/ground boundaries presented an accuracy of 94.3% and a precision of 100%. As a future study, the PGFA admittance method with phase/ground boundaries will be compared with protective relay's manufacturer methods with a real-time simulator and protective relays in the loop.

Abbreviations

PGFA: Phase-to-ground fault apparent
LEDs: Light-emitted diodes
AG: Phase A to ground
BCG: B-C to ground
CG: Phase C to ground
ABG: Phase A-B to ground
BG: Phase B to ground
CAG: Phase C-A to ground
PV: Photovoltaic
R-X: Resistance-reactance
LG: Line to ground
LLG: Double line to ground
LL: Line to line
3L: Three line
3LG: Three line to ground
EPB: Electric power board
COMTRADE: Common format for transient data exchange
CT/s: Current transformer/s
PT/s: Potential transformer/s
PRFS: Prefault state
FS: Fault state
POFS: Postfault state
NFS: Nonfault state

Symbols

Z_{ag}: PGFA impedance for phase A
V_a: Phase A to neutral voltage
I_a: Phase A current
I_b: Phase B current
I_c: Phase C current
I_0: Zero sequence current
K_0: Total zero sequence current compensation factor
Z_{T0}: Total zero sequence impedance
Z_{T1}: Total positive sequence impedance
$|K_0|$: Magnitude of the zero sequence current compensation factor for the power line sections
$K_{0<}$: Angle of the zero sequence current compensation factor for the power line sections
$K_{0\text{imag}}$: Imaginary part of the zero sequence current compensation factor magnitude
$K_{0\text{real}}$: Real part of the zero sequence current compensation factor magnitude
R_T: Total resistance of the power line sections
R_{T1}: Total positive sequence resistance of the power line sections
R_{T2}: Total negative sequence resistance of the power line sections
R_{T0}: Total zero sequence resistance of the power line sections
X_T: Total reactance of the power line sections
X_{T1}: Total positive sequence reactance of the power line sections
X_{T2}: Total negative sequence reactance of the power line sections
X_{T0}: Total zero sequence reactance of the power line sections
$|Y_T|$: Total admittance magnitude of the power line sections
$|Y_{T0}|$: Total zero sequence admittance magnitude of the power line sections
$|Y_{pg}|$: Phase-to-ground fault apparent admittance magnitude
$|Z_{T0}|$: Total zero sequence impedance magnitude of the power line sections
$|Z_{T1}|$: Total positive sequence impedance magnitude of the power line sections
$|Z_{T2}|$: Total negative sequence impedance magnitude of the power line sections
I_A: A phase current
I_B: B phase current
I_C: C phase current
V_A: A phase-to-ground voltage
V_B: B phase-to-ground voltage
V_C: C phase-to-ground voltage
Y_T: Total admittance
Y_{T0}: Total zero sequence admittance
Y_{AG}: A phase-to-ground fault apparent admittance
Y_{BG}: B phase-to-ground fault apparent admittance
Y_{CG}: C phase-to-ground fault apparent admittance
V_p: Generic phase-to-ground voltage
I_p: Generic phase current
Y_{pg}: Phase-to-ground fault apparent admittance
G_{pg}: Phase-to-ground fault apparent conductance
B_{pg}: Phase-to-ground fault apparent susceptance

θ_{pg}: Angle of the phase-to-ground fault apparent admittance
T_R: Relay time
TDS: Time dial setting
$I_{primary}$: Primary current
CTR: Current transformer ratio
I_P: Relay current pickup
R_{L1}: Positive sequence resistance of each power line section
X_{L1}: Positive sequence reactance of each power line section
R_{L0}: Zero sequence resistance of each power line section
X_{L0}: Zero sequence reactance of each power line section
TP: True positive
FP: False positive
TN: True negative
FN: False negative
Accuracy (%): Accuracy
Precision (%): Precision
Sensitivity (%): Sensitivity
Specificity (%): Specificity
Error rate (%): Error rate
$F_{sampling}$: Sampling frequency
F_{max}: Largest frequency component of the signal
T_{step}: Time step
S_{cycle}: Samples per cycle
Y: Measured admittance
I: Measured current
V: Measured voltage
$Error_{\%|Y|}$: Percentage admittance error
$Error_{\%|I|}$: Percentage current error
$Error_{\%|V|}$: Percentage voltage error.

Data Availability

The data supporting the results are included in Tables 4, 5, and 6 of the article.

Disclosure

This manuscript has been authored by UT-Battelle, LLC, under contract DE-AC05-00OR22725 with the US Department of Energy (DOE). The US government retains and the publisher, by accepting the article for publication, acknowledges that the US government retains a nonexclusive, paid-up, irrevocable, worldwide license to publish or reproduce the published form of this manuscript, or allow others to do so, for US government purposes. DOE will provide public access to these results of federally sponsored research in accordance with the DOE Public Access Plan (http://energy.gov/downloads/doe-public-access-plan).

Conflicts of Interest

The authors declare that there are no conflicts of interest regarding the publication of this paper.

Acknowledgments

This study was funded by the DarkNet project from the DOE at Oak Ridge National Laboratory.

References

[1] M. Hosseini, B. Stephen, S. D. J. McArthur, and J. Helm, "Current based trip coil analysis of circuit breakers for fault diagnosis," in *Proceedings of the 2018 IEEE PES Innovative Smart Grid Technologies Conference Europe (ISGT-Europe)*, Sarajevo, Bosnia and Herzegovina, October 2018.

[2] S. S. Biswas, A. K. Srivastava, and D. Whitehead, "A real-time data-driven algorithm for health diagnosis and prognosis of a circuit breaker trip assembly," *IEEE Transactions on Industrial Electronics*, vol. 62, no. 6, pp. 3822–3831, 2015.

[3] B. Kasztenny, M. V. Mynam, and N. Fischer, "Sequence component applications in protective relays – advantages, limitations, and solutions," in *Proceedings of the 46th Annual Western Protective Relay Conference*, Schweitzer Engineering Laboratories, Pullman, WA, USA, March 2019.

[4] D. Costello and K. Zimmerman, "Determining the faulted phase," in *Proceedings of the 63rd Annual Conference for Protective Relay Engineers*, Schweitzer Engineering Laboratories, College Station, TX, USA, March 2010.

[5] B. Zimmerman and D. Costello, "Impedance-based fault location experience," *SEL Journal of Reliable Power*, vol. 1, pp. 1–28, 2010.

[6] IEEE Standard C37 113-2015, *IEEE Guide for Protective Relay Applications to Transmission Lines*, IEEE, Piscataway, NJ, USA, 2016.

[7] D. D. Fentie, "Understanding the dynamic mho distance characteristic," in *Proceedings of the 69th Annual Conference for Protective Relay Engineers*, College Station, TX, USA, April 2016.

[8] IEEE Standard C37 2-2008, "IEEE standard electrical power system device function numbers, acronyms, and contact designations,", Piscataway, NJ, USA, October 2008.

[9] E. Godoy, H. J. Altuve, and N. Fischer, "Tutorial on single-pole tripping and reclosing," in *Proceedings of the 39th Annual Western Protective Relay Conference*, Spokane, WA, USA, October 2012.

[10] A. M. I. Haleem, M. Sharma, K. S. Sajan, and K. N. Dinesh Babu, "A comparative review of fault location/identification methods in distribution networks," in *Proceedings of the 2018 1st International Conference on Advanced Research in Engineering Sciences*, Dubai, UAE, June 2018.

[11] SEL-451-5 Protection, "Automation, and bay control system instruction manual," 2017, https://selinc.com/products/451/docs/.

[12] "SPAJ 142 C overcurrent and earth-fault relay, user's manual and technical description," 2002, https://library.e.abb.com/public/b3cb5ff579b5707dc2256bf1002cfb67/FM_SPAJ142C_EN_BAC.pdf.

[13] E. C. Piesciorovsky, T. Smith, and T. B. Ollis, "Protection schemes used in North American microgrids," *International Transactions on Electrical Energy Systems*, vol. 30, no. 9, pp. 1–28, 2020.

[14] Z. Q. Bo, B. R. J. Caunce, M. A. Redfern, and X. Z. Dong, "Under voltage accelerated protection of single source distribution systems," in *Proceedings of the 2003 IEEE Power Engineering Society General Meeting*, Toronto, ON, Canada, July 2003.

[15] US Patent 5, 325, 061 titled, "Computationally-efficient distance relay for power transmission lines," 1994, https://www.uspto.gov/.
[16] US Patent 5, 515, 227 titled, "Fault identification system for use in protective relays for power transmission lines," 1996, https://www.uspto.gov/.
[17] L. Wang, "The fault causes of overhead lines in distribution network," *MATEC Web of Conferences*, vol. 61, Article ID 02017, 2016.
[18] P. Liu and C. Huang, "Detecting single-phase-to-ground fault event and identifying faulty feeder in neutral ineffectively grounded distribution system," *IEEE Transactions on Power Delivery*, vol. 33, no. 5, pp. 2265–2273, 2018.
[19] "Distance protection," *Network Protection & Automation Guide*.
[20] S. B. Wilkinson and C. A. Mathews, "Dynamic characteristics of mho distance relays, GE power management," 2022, https://www.gegridsolutions.com/products/applications/ger3742.pdf.
[21] J. Roberts, A. Guzman, and E. O. Schweitzer, "Z = V/I does not make a distance relay," in *Proceedings of the 48th Annual Georgia Tech Protective Relaying Conference*, Atlanta, GA, USA, 1994.
[22] E. C. Piesciorovsky and A. G. Tarditi, "Modeling the impact of GIC neutral blocking devices on distance protection relay operations for transmission lines," *Electric Power Systems Research*, vol. 180, Article ID 106135, 2020.
[23] E. C. Piesciorovsky and M. F. Ferrari Maglia, "Comparison of high-speed adaptive and non-adaptive backup overcurrent protection on fuse feeders with sensors," *International Transactions on Electrical Energy Systems*, vol. 29, no. 4, Article ID e2812, 2018.
[24] E. C. Piesciorovsky and N. N. Schulz, "Comparison of programmable logic and setting group methods for adaptive overcurrent protection in microgrids," *Electric Power Systems Research*, vol. 151, pp. 273–282, 2017.
[25] X. Li, "Mathematical model for current transformer based on Jiles-Atherton theory and saturation detection method," Master's Thesis, University of Kentucky, Lexington, Kentucky, USA, 2016.
[26] F. Calero, "Distance elements: linking theory with testing," in *Proceedings of the Texas A & M Conference for Protective Relay Engineers*, College Station, TX, USA, March 2009.
[27] Everything about Data Science, "Confusion matrix," 2016, https://scaryscientist.blogspot.com/2016/03/confusion-matrix.html?view=classic.
[28] R. Silipo and M. Widmann, "Confusion matrix and class statistics," 2019, https://towardsdatascience.com/confusion-matrix-and-class-statistics-68b79f4f510b.
[29] S. Das, "Sub-Nyquist rate ADC sampling in digital relays and PMUs: advantages and challenges," in *Proceedings of the 6th IEEE International Conference on Power Systems*, New Delhi, India, March 2016.
[30] B. Kasztenny, "Settings considerations for distance elements in line protection applications," in *Proceedings of the 48th Annual Western Protective Relay Conference*, College Station, TX, USA, March 2021.
[31] F. B. Costa, B. A. Souza, and N. S. D. Brito, "Effects of the fault inception angle in fault-induced transients," *IET Generation, Transmission & Distribution*, vol. 6, no. 5, pp. 463–471, 2012.